JOURNAL OF VIROLOGY, Sept. 2005, p. 11335–11342 Vol. 79, No. 17
0022-538X/05/$08.00+0 doi:10.1128/JVI.79.17.11335–11342.2005

A Severe Acute Respiratory Syndrome-Associated Coronavirus-Specific Protein Enhances Virulence of an Attenuated Murine Coronavirus

Lecia Pewe,[1]† Haixia Zhou,[2]† Jason Netland,[1] Chandra Tangudu,[3] Heidi Olivares,[3] Lei Shi,[4] Dwight Look,[4] Thomas Gallagher,[3] and Stanley Perlman[1,2]*

Departments of Pediatrics,[1] Microbiology,[2] and Internal Medicine,[4] University of Iowa, Iowa City, Iowa 52242, and Department of Microbiology and Immunology, Loyola University Medical Center, Maywood, Illinois 60153[3]

Received 11 April 2005/Accepted 8 June 2005

Most animal species that can be infected with the severe acute respiratory syndrome-associated coronavirus (SARS-CoV) do not reproducibly develop clinical disease, hindering studies of pathogenesis. To develop an alternative system for the study of SARS-CoV, we introduced individual SARS-CoV genes (open reading frames [ORFs]) into the genome of an attenuated murine coronavirus. One protein, the product of SARS-CoV ORF6, converted a sublethal infection to a uniformly lethal encephalitis and enhanced virus growth in tissue culture cells, indicating that SARS-CoV proteins function in the context of a heterologous coronavirus infection. Furthermore, these results suggest that the attenuated murine coronavirus lacks a virulence gene residing in SARS-CoV. Recombinant murine coronaviruses cause a reproducible and well-characterized clinical disease, offer virtually no risk to laboratory personnel, and should be useful for elucidating the role of SARS-CoV nonstructural proteins in viral replication and pathogenesis.

Severe acute respiratory syndrome (SARS) was first identified in 2003 as a clinical entity with high morbidity and mortality, and soon thereafter, it was shown to result from infection with a novel coronavirus (SARS-CoV) (23). SARS-CoV causes the most severe illness of any human coronavirus identified thus far. However, several other coronaviruses, including transmissible gastroenteritis virus, infectious bronchitis virus, and feline infectious peritonitis virus, cause substantial morbidity and mortality in infected animals. In the most intensively studied coronavirus infection, rodents infected with neurotropic strains of mouse hepatitis virus (MHV) develop acute encephalitis and acute and chronic demyelinating diseases (30). MHV-induced demyelination is largely immune mediated. Immunodeficient mice (mice with severe combined immunodeficiency or deficient in recombination activation gene 1 activity) do not develop demyelination after infection with MHV. However, demyelination is detected a few days after transfer of anti-MHV T cells or antibodies (13, 16, 37) The immune response is also likely to contribute to clinical disease in humans with SARS, since disease worsened in some patients concomitant with virus clearance (24). SARS-CoV, like other coronaviruses, infects macrophages, which may also cause immune dysfunction (39). While these results suggest a role for the host response in SARS pathogenesis, study of the disease process has been limited by the absence of a reliable animal model. Mice, hamsters, ferrets, cats, and monkeys are susceptible to infection, but there is a lack of agreement between laboratories about the degree to which these animals exhibit clinical signs and pathological changes in infected organs (reviewed in reference 23). Few reagents are available to study the immune response except in mice, and immunocompetent mice do not develop clinical disease (32). Furthermore, work with live SARS-CoV requires a biosafety level 3 laboratory.

As an alternative to directly infecting animals with SARS-CoV, we engineered a set of recombinant MHVs that expressed individual SARS-CoV proteins. We reasoned that SARS-CoV proteins, particularly the nonstructural ones, would function in the context of MHV because MHV and SARS-CoV are both group 2 coronaviruses (10). Furthermore, several epidemiological and genetic studies have suggested that SARS-CoV crossed the species barrier from palm civet cats and other exotic animals to infect humans (24). These animals may not be the natural host for SARS-CoV; another animal, such as a rodent, might actually be the primary host. In either case, once SARS-CoV was able to infect across species lines, SARS-CoV proteins, including the nonstructural ones, would presumably function in the new host. The ability of SARS-CoV to infect several species of experimental animals also supports this notion. Recombinant MHV offers several advantages. First, MHV has been studied in multiple laboratories for many years, without any evidence of risk to laboratory personnel. Second, many laboratory strains, including the one used in our studies, pose no risk to uninfected mice since they do not spread to uninfected animals housed in the same cage (unpublished observations). Third, the innate and adaptive immune responses to MHV have been extensively investigated (11), and reagents are available to study the T- and B-cell responses to infection with recombinant MHV.

Our initial analyses were directed at investigating the role of SARS-CoV nonstructural proteins in murine disease. Like other coronaviruses, the SARS-CoV genome contains several novel open reading frames (ORFs) at the 3′ end of the genome. These ORFs are predicted to encode proteins that do not share homology with any other viral or cellular proteins.

* Corresponding author. Mailing address: Department of Pediatrics, University of Iowa, Medical Laboratories 2042, Iowa City, IA 52242. Phone: (319) 335-8549. Fax: (319) 335-8991. E-mail: Stanley-Perlman@uiowa.edu.

† L.P. and H.Z. contributed equally to the work.

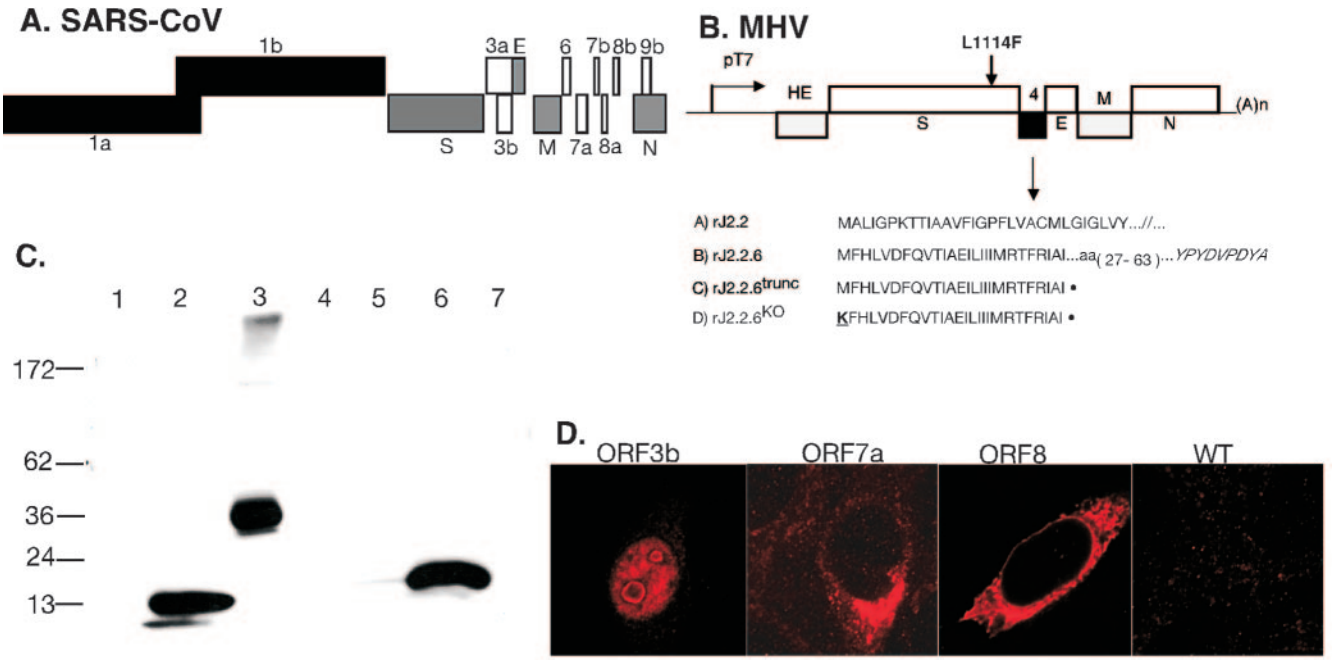

FIG. 1. Expression of SARS-CoV nonstructural ORFs in rJ2.2-infected cells. (A) Genome of SARS-CoV, with ORFs and structural proteins (gray). (B) SARS-CoV nonstructural proteins were introduced into rJ2.2 by targeted recombination (shown for rJ2.2.6) as described in Materials Methods. As controls, a termination codon was introduced at residue 27 in rJ.2.2.6^{trunc} and rJ2.2.6^{KO}. The initiator methionine was also mutated in rJ2.2.6^{KO}. Each construct was C terminus tagged with the influenza virus HA epitope. (C) The products of ORF3a, -6, and -7b were detected by Western blot analysis using anti-HA antibody. Lanes: 1, rJ2.2; 2, rJ2.2.6; 3, rJ2.2.3a; 4, rJ2.2.3b; 5, rJ2.2.7a; 6, rJ2.2.7b; 7, rJ2.2.8. (D) All of the inserted proteins were detected by IFA using anti-HA antibody. The products of ORF3b, -7a, and -8 are shown. Note that protein 3b was localized to the nucleus. No staining was detected in cells infected with rJ2.2 (WT).

Each coronavirus expresses a unique set of these nonstructural proteins. A general feature of coronavirus nonstructural proteins is that they are not required for growth in tissue culture cells (18). However, it is likely that they have a role in virus growth in infected animals. Identifying the functions of these viral proteins is challenging because, in some cases, their deletion has not affected the ability of viruses to cause acute disease (22). Here, we demonstrate that SARS-CoV nonstructural genes can be expressed in the context of the MHV genome and we also describe the initial characterization of a recombinant MHV expressing one of these proteins.

MATERIALS AND METHODS

Animals. Specific pathogen-free 5- to 6-week-old C57BL/6 (B6) mice (National Cancer Institute, Bethesda, MD) were inoculated intracranially (i.c.) with 1,000 PFU of virus in 40 μl of Dulbecco's modified Eagle's medium. Mice were examined and weighed daily. Mice were assessed for clinical disease using a previously described scale (5) as follows: 0, asymptomatic; 1, limp tail or slightly hunched; 2, wobbly gait or hunched or mild encephalitis; 3, hindlimb paresis or moderate encephalitis; 4, quadriparesis/paralysis or severe encephalitis; 5, moribund. In all experiments, mice were euthanized 21 days postinfection (p.i.). Virus was harvested from the infected central nervous systems (CNS), and titers were determined by plaque assay on HeLa cells expressing the cellular receptor for mouse hepatitis virus (HeLa-MHVR). All animal studies were approved by the University of Iowa Animal Care and Use Committee.

Viruses and cells. Virus was grown in 17Cl-1 cells, and titers were determined on HeLa-MHVR cells. Murine 17Cl-1 and L929 cells and human HeLa-MHVR cells were infected with recombinant MHV. In all experiments in which virus titers were measured, cells and supernatants were combined prior to titer determinations.

Recombinant viruses. Targeted recombination (17, 22) was used to generate recombinant virus expressing individual SARS-CoV nonstructural proteins (Fig. 1A and B). Briefly, PCR products corresponding to nucleotides 25268 to 26092 (ORF3a), 25689 to 26153 (ORF3b), 27074 to 27265 (ORF6), 27273 to 27641 (ORF7a), 27638 to 27772 (ORF7b), and 27779 to 27898 (ORF8) were generated by reverse transcription-PCR (RT-PCR) using RNA harvested from cells infected with the Urbani strain of SARS-CoV (GenBank accession number AY278741; kindly provided by Tom Ksiazek, Centers for Disease Control and Prevention, Atlanta, GA). The ORF8 product was further modified by addition of the 29-nucleotide sequence present in some SARS-CoV strains but absent from the Urbani strain (3). The reverse primers also encoded an influenza hemagglutinin (HA) epitope to monitor expression. PCR products were inserted into gene 4 of a plasmid containing genes 2 to 9 of the neuroattenuated J2.2-v-1 variant of MHV (8, 16) (Fig. 1). Strain J2.2-v-1 differs from neurovirulent strain JHM.SD by a single mutation in the S protein (L1114F), as indicated in Fig. 1 (15, 35). Donor RNAs were transcribed using T7 polymerase and transfected into feline cells (AK-D) previously infected with fMHV-JHM (a recombinant MHV strain encoding the feline surface [S] glycoprotein [22]). fMHV-JHM does not infect murine cells, but recombinant virus expressing the MHV S protein does, allowing for efficient selection of recombinant virus on 17Cl-1 murine cells. As controls for studies of the recombinant virus encoding ORF6 (rJ2.2.6), a second set of viruses was engineered in which a termination codon was introduced at amino acid 27 using overlapping extension PCR (pJ2.2.6^{trunc}). As another control, viruses were also developed in which the ORF6^{trunc} initiator methionine was mutated to lysine (J2.2.6^{KO}). The presence of the introduced SARS-CoV RNA was confirmed by sequence analysis prior to use in further studies. To control for any unwanted mutations that might have occurred during the process of targeted recombination, at least two independent isolates of each recombinant virus were analyzed in these studies. Identical results were obtained with both isolates, and data from both isolates were combined in the studies described below. In addition, S genes of recombinant virus isolates rJ2.2, rJ.2.2.6.1, and rJ2.2.6^{KO} were sequenced and found to be identical to the plasmid sequence, thereby ruling out spurious mutations in S that might influence virulence.

Western blot analysis. 17Cl-1 cells infected with recombinant MHV expressing SARS-CoV proteins (multiplicity of infection [MOI] = 1) were harvested at 16 h p.i. HA-tagged SARS-CoV proteins were detected by immunoblot analysis, using

a biotinylated rat anti-HA antibody (monoclonal antibody [MAb] 3F10; Roche Molecular Biochemicals, Mannheim, Germany) and streptavidin-horseradish peroxidase (Jackson Immunoresearch, West Grove, PA). Protein was detected using an ECLplus detection kit (Amersham Biosciences, Piscataway, NJ).

Immunofluorescence assays. 17Cl-1 cells infected with recombinant MHV were fixed at 8 to 9 h p.i. with methanol. SARS-CoV proteins were detected using anti-HA murine antibody (MAb HA.11; Covance, Berkeley, CA), biotinylated goat anti-mouse Ab (Jackson Immunoresearch), and streptavidin-Cy3 (Jackson Immunoresearch). To localize the ORF6 protein, L929 cells were infected with rJ2.2.6 and fixed at 12 to 16 h p.i. Samples were doubly stained for the ORF6 protein (MAb 3F10, biotin conjugated; Roche) and an endoplasmic reticulum protein (BiP; MAb 10C3; Stressgen Bioreagents, Victoria, CA) or MHV structural proteins (transmembrane [M] MAb 5B11.5, surface [S] MAb 4B11.6, and nucleocapsid [N] MAb 5B188.2) (all provided by M. Buchmeier, The Scripps Research Institute, La Jolla, CA). Cells were then incubated with fluorescein isothiocyanate-conjugated donkey anti-mouse Ab (Jackson Immunoresearch) and a TSA-Cy3 amplification kit (Perkin-Elmer, Boston, MA).

Real-time RT-PCR. Total RNA was isolated from brains using Tri reagent (Molecular Research Center, Inc., Cincinnati, OH) following the manufacturer's instructions. cDNA was synthesized as previously described (26). Two microliters of cDNA was added to a 23-μl PCR cocktail containing 2× SYBR Green Master Mix (ABI, Foster City, CA) and 0.2 μM of each sense and antisense primer (IDT DNA, Coralville, IA). Amplification was performed in an ABI Prism7700 thermocycler. Specificity of the amplification was confirmed using melting curve analysis. Data were collected and recorded by ABI Prism 7700 software and expressed as a function of the threshold cycle (*Ct*), the cycle at which the fluorescence intensity in a given reaction tube rises above background (calculated as 10 times the mean standard deviation of fluorescence in all wells over the baseline cycles). Specific primer sets used for MHV-JHM and the murine housekeeping gene were as follows (5′ to 3′); JHM nucleocapsid sense, GACACAA CCGACGTTCCTTT; JHM nucleocapsid antisense, TAGCAGGTGCAGACC TTCCT; hypoxanthine phosphoribosyltransferase (HPRT) sense, CCTCATGG ACTGATTATGGAC; HPRT antisense, CAGATTCAACTTGCGCTCATC. Quantitative JHM nucleocapsid (N) abundance was calculated as follows: for each cDNA sample assayed, *Ct* values for reactions amplifying JHM nucleocapsid and HPRT were determined. JHM N *Ct* values for each sample were corrected by subtracting the *Ct* for HPRT (Δ*Ct*). The ratio of JHM N RNA to HPRT RNA was calculated by the formula $2^{-(\Delta Ct)}$. The validity of this approach was confirmed by using serial 10-fold dilutions of cDNA. The amplification efficiencies for JHM nucleocapsid antisense and murine HPRT amplimers were found to be identical.

Metabolic radiolabeling and immunoprecipitation assays. Eighty percent confluent L929 or HeLa-MHVR cells were infected with recombinant MHV (MOI = 1). At the indicated times, the cells were washed, placed into methionine-free medium, and labeled for 30 min with 50 μCi of Trans^{35}S-label (ICN Biomedicals, Inc., Aurora, Ohio). Cell lysates were prepared as previously described (20). MHV proteins were immunoprecipitated with rabbit anti-MHV antibody and antigen-antibody complexes collected onto protein A-Sepharose beads (Amersham Pharmacia Biotech AB, Uppsala, Sweden). Samples were analyzed by polyacrylamide gel electrophoresis.

To assess whether ORF6 was virion associated, supernatants from infected cells were centrifuged at 2,000 × *g* at 5°C to remove debris and then at 20,000 × *g* for 10 min at 5°C. Clarified medium was overlaid onto linear 3-ml 10-to-30% (wt/wt) sucrose gradients in HNB (25 mM sodium HEPES [pH 7.4], 100 mM NaCl, 0.1% bovine serum albumin). Centrifugation was performed at 5°C in an SW60 rotor for 1 h at 55,000 rpm. The gradient was decanted, and pellets containing intact virions were dissolved in 0.1 ml of sodium dodecyl sulfate lysis buffer (62 mM Tris HCl [pH 6.8], 2% sodium dodecyl sulfate, 5% 2-mercaptoethanol, 2.5% Ficoll, 0.01% bromphenol blue) prior to gel electrophoresis and subsequent immunoblotting for the HA-tagged ORF6 protein.

Northern blot analysis. RNA was prepared from L929 cultures infected with recombinant MHV at 16 h p.i. and from mock-infected cultures and analyzed as previously described (22).

Flow cytometry. Leukocytes were harvested from the infected CNS (25) and analyzed for neutrophils, macrophages, and MHV-specific CD4 T cells and CD8 T cells. Briefly, mice were perfused with phosphate-buffered saline and brains and spinal cords were removed. Tissue was ground between frosted glass slides and triturated by vigorous pipetting in 5 ml of RPMI medium with 10% fetal calf serum. Following thorough dispersion of the tissue, Percoll (Pharmacia, Uppsala, Sweden) was added to a final concentration of 30%. The lysate was spun at 1,300 × *g* for 30 min at 4°C. The Percoll and lipid layers were aspirated, and the cell pellet was washed and counted. Antibodies used for phenotyping cells were biotinylated rat anti-mouse F4/80 (cl BM-8; Caltag Laboratories, Burlingame, CA), peridinin chlorophyll protein-conjugated rat anti-mouse CD45 (BD Biosciences, San Diego, CA), and fluorescein isothiocyanate-labeled rat anti-mouse Ly6G (MAb 1A8; BD Biosciences). In all cases, isotype-matched control antibodies were used. MHV-specific CD4 and CD8 T cells were identified using an intracellular gamma interferon (IFN-γ) detection assay as described previously (36). Samples were analyzed on a FACScan flow cytometer (BD Biosciences, Mountain View, CA).

IFN-α/β bioassay. Levels of IFN-α/β were assayed using a bioassay based on inhibition of vesicular stomatitis virus (VSV) growth in L929 cells. L929 cells were infected with recombinant MHV at an MOI of 0.1. Supernatants were harvested, and MHV was UV inactivated. L929 cells infected with 1,000 PFU of VSV were treated at 30 min p.i. with dilutions of supernatants or recombinant murine IFN-β (PBL Biomedical Laboratories, Piscataway, NJ). Titers of VSV were determined on Vero cells. IFN-α/β levels were calculated based on the standard curves generated with recombinant IFN. To verify production of IFN by L929 cells, samples were treated with 25 μg poly(I-C) (Invivogen, San Diego, CA) and supernatants were assayed.

Sensitivity to IFN-β. The relative sensitivities of rJ2.2.6 and rJ2.2.6^{KO} to IFN-β were measured by treating infected L929 cells with serial dilutions of IFN-β. IFN-β was added 30 min p.i.; in some experiments, cells were also pretreated with the same concentration of IFN-β for 24 h. MHV titers were determined on HeLa-MHVR cells. As a control, VSV-infected L929 cells were treated in parallel with IFN-β and virus titer was determined on Vero cells.

Retrovirus constructions. ORF6-HA was cloned into pBMN-IRES-GFP and transfected into Phoenix-Eco cells (provided by G. Nolan, Stanford University) using calcium-phosphate precipitation (Nolan Laboratory website protocols). Retroviral particles were harvested and transduced into L929 cells using Polybrene. After two passages, green fluorescent protein-positive (GFP$^+$) cells were sorted by flow cytometry. The presence of the ORF6-HA protein was confirmed by indirect immunofluorescence assay (IFA) using anti-HA antibody.

Statistics. A two-tailed unpaired Student's *t* test was used to analyze differences in mean values between groups. All results are expressed as means ± standard errors of the means (SEM). *P* values of <0.05 were considered statistically significant.

RESULTS

Development and analysis of recombinant MHV expressing SARS-CoV nonstructural proteins. We chose the well-characterized attenuated rJ2.2 variant of MHV as the substrate for developing recombinant virus. Previously, we showed that insertion of exogenous genes into ORF4 of MHV did not affect its abilities to grow in tissue culture cells or cause acute neurological disease in mice (22). Consequently, we inserted SARS-CoV-specific ORFs 3a, 3b, 6, 7a, 7b, and 8 into this site. In each case, an HA epitope tag was inserted at the 3′ end of the sequence to facilitate detection. ORF6-HA, ORF3a-HA, and ORF7b-HA (but not ORF-3b, ORF-7a, and ORF-8) were detected by immunoblot assay (Fig. 1C). All six proteins were detected by IFA in the cytoplasm of infected cells except for ORF3b-HA, which was localized to the nucleus (Fig. 1D). Next, we inoculated B6 mice with 1,000 PFU of each recombinant virus as well as rJ2.2 and monitored clinical outcomes. Preliminary analyses showed that infection with rJ2.2.6 (MHV expressing ORF6-HA) resulted in greater morbidity and mortality than did infection with any of the other recombinant viruses or with rJ2.2. Based on these results, we analyzed infection with rJ2.2.6 in more detail. Of note, the ORF6 protein is completely conserved in all SARS-CoV isolates and shares no homology with any known viral or cellular proteins. The sequence of the ORF6 protein suggests that it is membrane associated.

ORF6 protein expression converts a sublethal to a lethal infection. As a control for experiments with rJ2.2.6, we engineered a second set of recombinant viruses in which a termination codon was introduced at amino acid 27 (rJ2.2.6^{trunc}) as

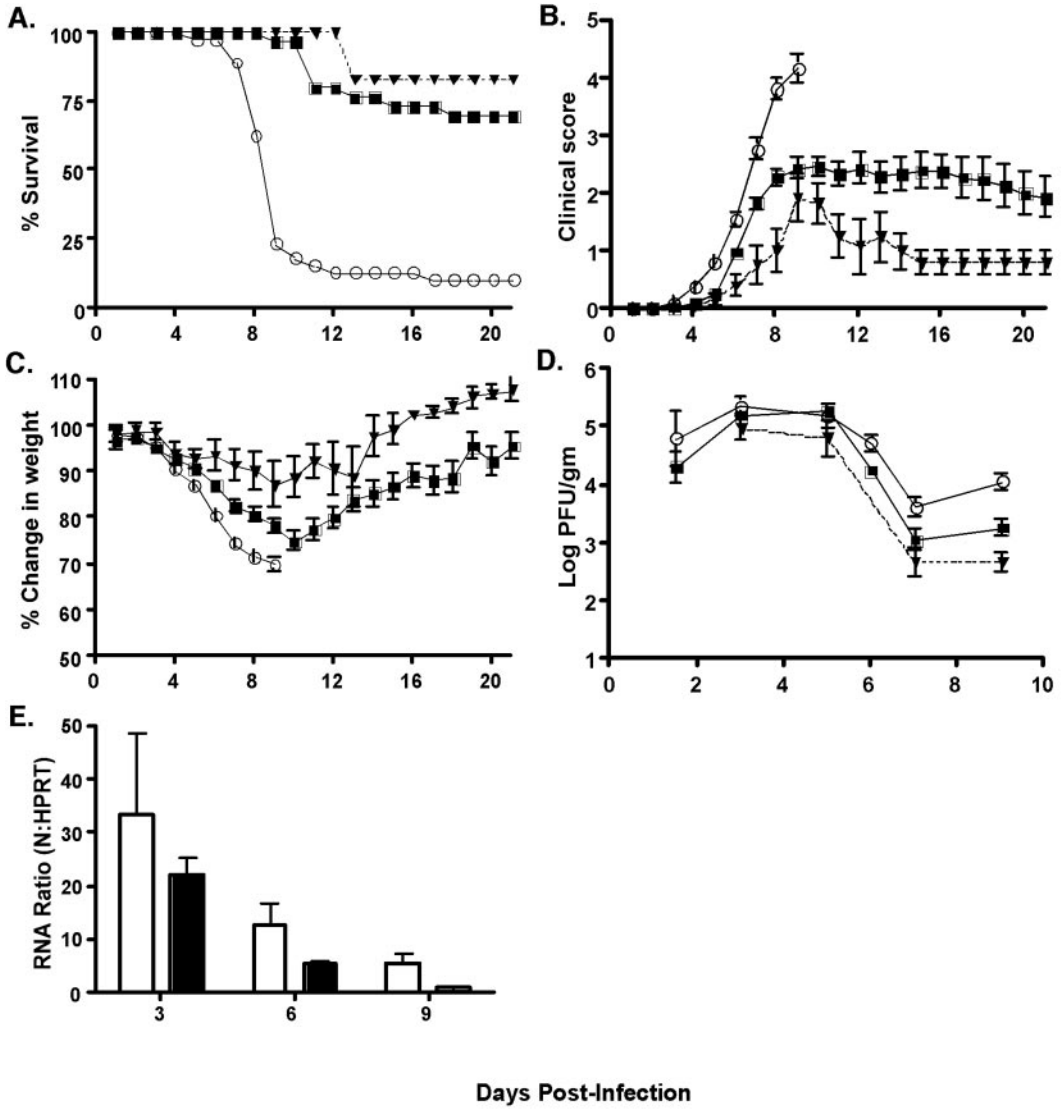

FIG. 2. Mortality, morbidity, and virus titers in mice infected with rJ2.2.6, rJ2.2.6^{trunc}, or rJ2.2.6^{KO}. Mice were infected with rJ2.2 (triangles), rJ2.2.6 (open circles), or rJ2.2.6^{trunc} or rJ2.2.6^{KO} (squares) and monitored for mortality (A), clinical disease (B), and weight loss (C). Groups of 6 rJ2.2-, 38 rJ2.2.6-, and 30 rJ2.2.6^{trunc}- or rJ2.2.6^{KO}-infected mice were used in these studies. (D) CNS virus titers were also determined. A total of 212 mice were used for this purpose. Significant increases in virus titers were detected in the CNS of rJ2.2.6-infected mice compared to mice infected with rJ2.2.6$^{trunc+KO}$ (day 1.5, $P = 0.38$; day 3, $P = 0.23$; day 6, $P < 0.01$; day 7, $P = 0.056$; day 9, $P < 0.001$). Significant increases in virus titers were detected in the CNS of rJ2.2.6-infected mice compared to mice infected with rJ2.2 (day 7, $P < 0.05$; day 9, $P < 0.005$). Data for days 0 to 9 p.i. are shown in panels B, C, and D for the rJ2.2.6-infected mice because only 23% of mice survived past this time. The data for rJ2.2.6^{trunc}- and rJ2.2.6^{KO}-infected mice were combined, since mice infected with these viruses developed the same clinical disease. (E) RNA was harvested from the brains of mice infected with rJ2.2.6 (open bars; $n = 3$) or rJ2.2.6^{KO} (closed bars; $n = 3$) at each time point. The amount of N gene-specific RNA was quantified by real-time RT-PCR as described in Materials and Methods.

well as a third set which contained the terminator codon and a mutated initiator codon (methionine to lysine) (rJ2.2.6^{KO}). For all experiments, two independent isolates of each recombinant virus were analyzed to control for any mutations introduced during the recombination process. We infected B6 mice with 1,000 PFU of each recombinant virus by i.c. inoculation and monitored animals for weight loss, clinical signs, and death. We combined the results obtained with the rJ2.2.6^{trunc} and rJ2.2.6^{KO} (labeled rJ2.2.6$^{KO+trunc}$ in the figure) because they were indistinguishable. Mice infected with rJ2.2.6 developed clinical disease and lost weight at earlier times p.i. than did those infected with rJ2.2 or rJ2.2.6$^{KO+trunc}$ (Fig. 2B and C). Further, over 75% of rJ2.2.6-infected mice died by day 9 p.i.; in contrast, 70% or 83% of mice infected with rJ2.2.6$^{KO+trunc}$ or rJ2.2 survived until sacrifice at day 21 (Fig. 2A). Increased mortality in rJ2.2.6-infected mice correlated with higher virus titers (Fig. 2D), although significant differences in titers were only observed at >6 days p.i. compared to mice infected with rJ2.2.6$^{KO+trunc}$. These results were confirmed when virus-specific RNA levels in the brain were determined by Northern blot analysis (data not shown) or real-time PCR (Fig. 2E).

TABLE 1. Frequencies and numbers of macrophages and neutrophils in the CNS

Virus and group (n)[a]	Starting no. (10^5)	Macrophages		Neutrophils	
		%	No. (10^4)	%	No. (10^4)
rJ2.2.6					
Day 1.5 (6)	7.5 ± 1.3	47.2 ± 4.9	7.8 ± 2.7	9.7 ± 1.5	1.4 ± 0.3
Day 3 (6)	7.5 ± 1.0	33.6 ± 3.3	14 ± 3.0	32.6 ± 5.3[b]	12 ± 3.0[b]
Day 6 (4)	12 ± 2.0	12.7 ± 0.8	7.6 ± 2.2	4.8 ± 1.0[b]	2.5 ± 0.4[b]
rJ2.2.6$^{trunc\&KO}$					
Day 1.5 (6)	4.5 ± 0.6	42.6 ± 2.6	4.7 ± 1.0	12.8 ± 2.7	1.6 ± 0.6
Day 3 (10)	5.8 ± 0.8	32.7 ± 2.8	6.7 ± 2.3	14.7 ± 2.5	2.7 ± 0.9
Day 6 (6)	13 ± 1.0	21.2 ± 2.9	16 ± 3.0	2.5 ± 0.3	1.8 ± 0.2

[a] Number of individual mice analyzed.
[b] Increased neutrophils (frequency and number) were present in the rJ2.2.6-infected CNS at day 3 ($P < 0.005$) and day 6 p.i. ($P < 0.05$ for the frequency; $P = 0.13$ for the number). Values are means ± SEM.

Infection with rJ2.2.6 resulted in increased neutrophil infiltration. These results demonstrated that ORF6-HA protein, in the context of rJ2.2, resulted in greatly enhanced clinical disease and death compared to control viruses. We postulated that the ORF6 protein might enhance MHV growth or, alternatively, might inhibit the innate or adaptive antiviral immune response. Initially, we studied the effect of ORF6-HA on the murine inflammatory cellular response to MHV in individual mice by histological examination and by using flow cytometry. We did not detect substantial differences in the extent of inflammatory cell infiltration when sections from infected mice were examined after staining with hematoxylin and eosin. Cells were harvested from the infected CNS at 1.5, 3, and 6 days p.i. and neutrophils ($CD45^{hi}$ $F4/80^{-}$ $Ly6G^{+}$) and macrophages ($CD45^{hi}$ $F4/80^{+}$) were enumerated as described in Materials and Methods. We detected statistically significant increases in frequency (days 3 and 6 p.i.) and in number (day 3 p.i.) of neutrophils in the brains of mice infected with rJ2.2.6 compared to those of mice infected with rJ2.2.6$^{KO+trunc}$ (Table 1).

The anti-MHV T-cell responses in B6 mice are directed in large part at two CD8 T-cell epitopes (spanning residues 510 to 518 [epitope S510] and 598 to 605 of the S protein) and a single immunodominant CD4 T-cell epitope (encompassing residues 134 to 147 of the M protein [epitope M134]) (1, 2, 38). When CD4 and CD8 T-cell responses were analyzed, fewer numbers of epitope-specific cells were detected in the CNS of mice infected with rJ2.2.6 than in those infected with rJ2.2.6$^{KO+trunc}$, but these differences were not statistically significant (Table 2). Collectively, these results show that the presence of the ORF6 protein increased neutrophil infiltration into the CNS to a significant extent but did not significantly affect the T-cell response.

Infection with rJ2.2.6 resulted in increased virus growth in tissue culture cells. To investigate a role for the ORF6 protein in either enhancing virus growth or in inhibiting the innate immune response, we infected 17Cl-1, L929, and HeLa-MHVR cells with rJ2.2.6, rJ2.2.6^{KO}, or rJ2.2. 17-Cl-1 and HeLa-MHVR cells are very susceptible to infection with MHV, whereas L929 cells are much less susceptible. In all cases, infection with rJ2.2.6 resulted in more rapid development of cytopathic changes than did infection with any of the control viruses. However, the differences in L929 were most striking, in part because the kinetics of MHV infection in this cell line were slower than was observed with the other two cell lines. Infection of L929 cells with rJ2.2.6 resulted in the earlier appearance of syncytia, with concomitant increased virus titers detected up to 48 h p.i. (Fig. 3A) compared to cells infected with rJ2.2.6^{KO}. Viral RNA and protein levels were also increased in L929 cells infected with rJ2.2.6 compared to those infected with rJ2.2.6^{KO} (Fig. 3B and C). The same results were obtained with two different isolates of rJ2.2.6 and rJ2.2.6^{KO} (Fig. 3C).

L929 cells have intact IFN-α/β production and signaling pathways. Since SARS-CoV inhibits IFN-β expression (29) and SARS-CoV replication is only inhibited modestly by IFN-α/β treatment (4, 12, 27, 31), we next assessed whether inhibition of either IFN-α/β induction or signaling by ORF6-HA could contribute to the increased lethality observed in rJ2.2.6-infected mice. First, IFN-α/β levels in the supernatants of cells infected with rJ2.2.6 or rJ2.2.6^{KO} were measured using a bioassay, as described in Materials and Methods. Consistent with a previous report (9), neither recombinant MHV induced IFN-α/β (<1 U/ml), while treatment with poly(I-C) resulted in significant induction of IFN-α/β (143.6 ± 9 U/ml). Second, cells were treated with various concentrations of IFN-β prior to and after infection with rJ2.2.6 or rJ2.2.6^{KO}. Both viruses showed similar patterns of inhibition by IFN-β, although titers of rJ2.2.6 were consistently higher than those of rJ2.2.6^{KO} at every concentration of IFN-β that was analyzed (Fig. 3D).

These results do not show that the primary effect of ORF6-HA is to inhibit IFN production or signaling. In several other infections, viral proteins inhibit host cell protein synthesis by inactivating specific translation initiation factors. In turn, viruses have developed mechanisms, such as the use of an internal ribosome entry site, to enhance translation of viral proteins in the absence of the inactivated factors. To determine whether ORF6-HA inhibited host cell protein synthesis, we infected HeLa-MHVR cells with rJ2.2.6 or rJ2.2.6^{KO} and determined the effect on protein synthesis using [^{35}S]methionine-cysteine pulse-labeling and polyacrylamide gel electrophoresis. The presence of the ORF6 protein did not affect the amount of residual host protein synthesis present at 4, 8, or 12 h p.i. (data not shown).

Collectively, these results are consistent with the notion that

TABLE 2. Number of MHV epitope-specific CD4 and CD8 T cells in the CNS (day 7 p.i.)

Virus (n)[a]	% CD8	Epitope S510 (CD8)		% CD4	Epitope M134 (CD4)	
		%	No. (10^4)		%	No. (10^4)
rJ2.2.6 (8)	32.7 ± 3.2[b]	10.8 ± 1.3	3.8 ± 0.6	15.0 ± 1.7	5.3 ± 0.9	0.7 ± 0.1
rJ2.2.6$^{trunc\&KO}$ (6)	26.4 ± 3.2	15.7 ± 2.5	4.8 ± 1.6	15.4 ± 3.7	6.7 ± 1.3	1.2 ± 0.6

[a] Number of individual mice analyzed.
[b] Values are means ± SEM.

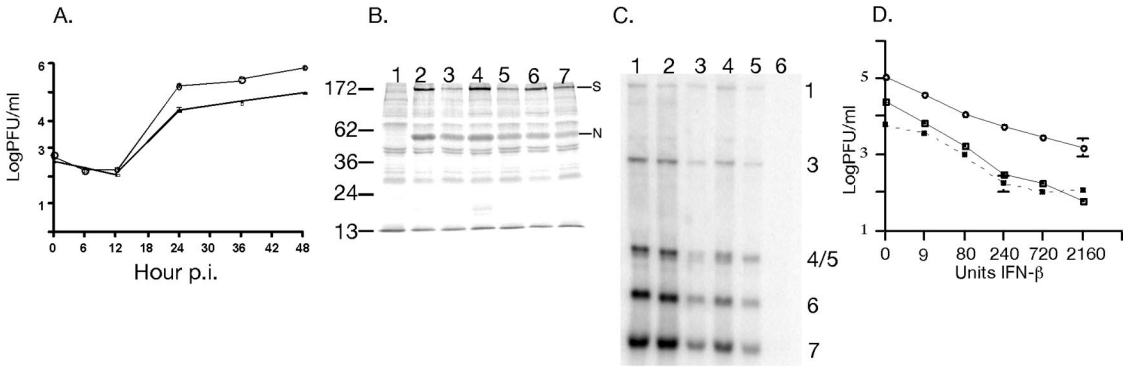

FIG. 3. Virus titers and interferon responses in rJ2.2.6- and rJ2.2.6^{KO}-infected L929 cells. (A) L929 cells were infected with rJ2.2.6 or rJ2.2.6^{KO} at an MOI of 1. Cells were harvested in triplicate at the indicated times, and virus titers were measured on HeLa-MHVR cells. Open circles, rJ2.2.6; squares, rJ2.2.6^{KO}. Titers and SEM are shown. (B) L929 cells infected with rJ2.2.6 (lanes 2, 4, and 6) or rJ2.2.6^{KO} (lanes 3, 5, and 7) were pulse-labeled with Tran^{35}S-label for 30 min at 17 h (lanes 2 and 3), 22 h (lanes 4 and 5), and 29 h (lanes 6 and 7) and processed as described in Materials and Methods. Lane 1 shows mock-infected cells. The N and S proteins are indicated. Fifty micrograms of protein was loaded per lane. (C) RNA was harvested at 16 h p.i. from L929 cells infected with rJ2.2.6 (lanes 1 and 2; two isolates), rJ2.2.6^{KO} (lanes 3 and 4; two isolates), or rJ2.2 (lane 5) or mock-infected cells (lane 6) and analyzed as described in Materials and Methods. Ten micrograms of RNA was loaded per lane. Viral RNAs 1 (genomic) and 2 to 7 (subgenomic) are indicated on the right. (D) At 24 h prior to infection with rJ2.2 (dashed line), rJ2.2.6 (open circles), or rJ2.2.6^{KO} (squares), cells in triplicate were treated with the indicated concentrations of IFN-β. After infection (MOI = 0.1), cells were then incubated for 20 h in the presence of the same concentration of IFN. Samples were then harvested and virus titers were determined on HeLa-MHVR cells.

ORF6, in the context of infection with MHV, directly enhances virus growth in infected cells. We determined that the ORF6 product was not preferentially incorporated into virions (Fig. 4), making it unlikely to act by augmenting the specific infectivity of secreted particles. Since coronavirus replication and assembly occur on cellular membranes and the primary structure of ORF6 suggests that it is membrane associated, we next determined whether ORF6-HA colocalized with any of the major MHV structural proteins or with a marker for the endoplasmic reticulum (BiP) (Fig. 5). The MHV M protein is localized to the Golgi in infected cells and serves as a marker for this structure (18). ORF6-HA was broadly distributed throughout the cytoplasm. L929 cells transduced with a retrovirus expressing ORF6-HA showed a similar pattern, suggesting that the ORF6 protein does not require any other viral proteins for intracellular localization. The merged composite figures showed strongest colocalization with the M protein, but there was significant overlap with the S, N, and BiP proteins as well. This labeling suggests that ORF6-HA is associated with membranes throughout the cell, although the majority is present in the endoplasmic reticulum and Golgi compartments.

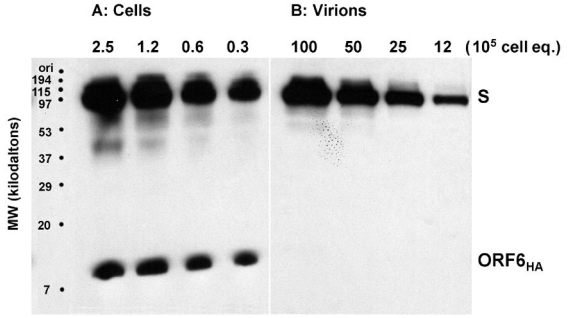

FIG. 4. Distribution of S and ORF6-HA proteins in infected cell cultures. 17Cl-1 cells infected with rJ2.2.6 (MOI = 0.05) were detergent solubilized at 24 h p.i. (A) The indicated number of cell equivalents were subjected to electrophoresis and immunoblotting using MAb 10G (kindly provided by F. Taguchi, National Institute of Neuroscience, Tokyo, Japan) and anti-HA MAb HA.11 (Covance, Inc.) to detect S and ORF6-HA, respectively. (B) Virions were concentrated from clarified media by pelleting through sucrose cushions as described in Materials and Methods, and proteins were similarly processed to reveal the proteins. S proteins were distributed in a ~40:1 cell/virion ratio, while ORF6-HA proteins were distributed in a >300:1 cell/virion ratio.

We performed additional studies to confirm ORF6-HA association with membranes. Bioinformatic analyses suggested that ORF6 amino acid residues 7 to 37 were predominantly hydrophobic. As several charged residues (E13, R20, R23, and D30) intersperse this otherwise-hydrophobic stretch, residues 7 to 37 may not form a bona-fide transmembrane span, but they may be sufficient to position ORF6 at membrane interfaces. To determine whether ORF6-HA exhibits a hydrophobic character, we partitioned infected cell proteins into hydrophobic and hydrophilic phases using a method involving TX-114 detergent. Our results (Fig. 6) revealed that ORF6-HA partitioned exclusively in the hydrophobic detergent phase. By contrast, over 90% of MHV N proteins segregated into the hydrophilic aqueous phase, while triple membrane-spanning M proteins were retained with ORF6-HA in the hydrophobic environment.

DISCUSSION

Our results show that SARS-CoV nonstructural proteins can function in the context of a heterologous murine coronavirus infection. The strain of MHV used in these experiments infects only the CNS and does not cause respiratory disease. Thus, these recombinant viruses are most useful for studying SARS-CoV-specific nonstructural proteins generally involved in

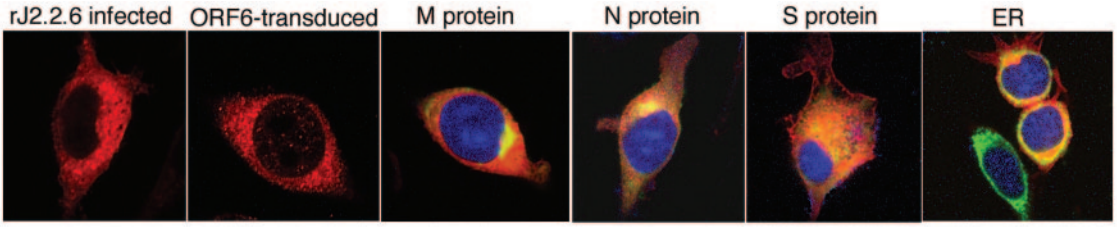

FIG. 5. Localization of ORF6-HA with MHV structural proteins and BiP. L929 cells were infected with rJ2.2.6 for 12 to 16 h. After fixation, cells were stained for HA and the MHV M, N, and S proteins or the endoplasmic reticulum (ER) protein BiP. L929 cells transduced with a retrovirus expressing ORF6-HA are also shown. The last four panels are merged to show colocalization of ORF6-HA with the indicated protein.

pathogenesis and not functions of these proteins that are specific for the respiratory tract. Of note, although patients who survive infection with SARS-CoV often develop psychiatric sequelae, SARS does not commonly infect the CNS (24).

We have also demonstrated, for the first time for any coronavirus, that one of the nonstructural proteins has a role in enhancing virus virulence in an animal host. The ability of the SARS-CoV protein to function in a nonhuman cell is not surprising. SARS-CoV most likely spread from infected exotic animal species, such as palm civet cats, to humans (24). Once SARS-CoV acquired the ability to infect human cells, consistent changes during the 2003 epidemic were detected only in the S, ORF3a, and nsp3 proteins (28). Notably, the ORF6 protein did not mutate after passage in humans.

While our results clearly show that ORF6-HA increased the lethality of infection in mice and enhanced virus growth in tissue culture cells, they did not demonstrate any inhibitory effect on the innate or adaptive cellular immune response or any change in virus susceptibility to IFN-β treatment. In addition, we could not demonstrate an effect on the induction of IFN-responsive genes, such as ICAM-1 and 2′-5′ oligoadenylate synthetase (unpublished data). Both MHV and SARS-CoV inhibit IFN induction (references 9 and 29 and our results), making it impossible to determine any effect that the ORF6 protein might have in this process. Although the ORF6 protein increased virus titers 10-fold in tissue culture cells, the effects on titers in infected mice were much less profound, with statistically significant differences detected only at later times p.i. (Fig. 2D). However, these differences may have caused an increase in the number of infiltrating neutrophils (Table 1) which, in turn, may have contributed to more severe disease.

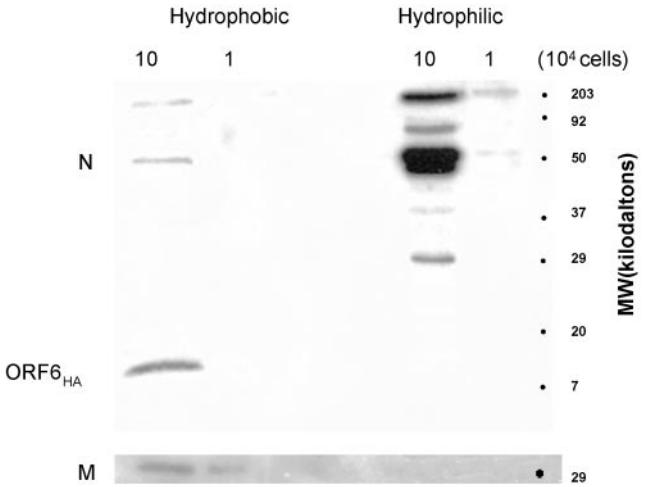

FIG. 6. Partitioning of MHV N, M, and ORF6-HA proteins into hydrophobic and hydrophilic environments. 17Cl-1 cells infected with rJ.2.2.6 were collected at 16 h p.i., and proteins were partitioned into hydrophobic (Triton X-114 detergent) and hydrophilic (aqueous) phases, using M-PER reagents (Pierce Company, Rockford, IL). Proteins from the indicated cell equivalents were then subjected to sodium dodecyl sulfate-polyacrylamide gel electrophoresis, transferred to polyvinylidene difluoride membranes, and probed simultaneously with anti-N MAb 5A5.2 and Covance anti-HA MAb 1.1 (top panel). The blot was then stripped and reprobed with anti-M MAb 4B6.2 (bottom panel).

Alternatively, the ORF6 protein may preferentially affect growth in a specific cell type, such as macrophages or dendritic cells, with consequent immune dysregulation. MHV is known to replicate in both cell types (30, 34) (data not shown). Macrophages and, most likely, dendritic cells are also infected in cats carrying another coronavirus, feline infectious peritonitis virus. Infection of these cells contributes to the progressive, relapsing disease associated with immunosuppression, elevated levels of proinflammatory cytokines and chemokines, and significant morbidity and mortality observed in infected cats (6). We did not detect substantial differences in levels of CCL2, CCL3, CCL4, CCL5, CCL7, CXCL10, tumor necrosis factor alpha, or interleukin-1β in the CNS of rJ2.2.6- and rJ2.2.6^{KO}-infected mice by RNase protection assays (data not shown), but this type of assay would not detect localized, but important, differences in chemokine or cytokine levels. In mice infected with influenza virus, fairly subtle differences in virus titers at early times p.i. create significant effects on dendritic cells and in the subsequent T-cell response, thus distinguishing lethal from nonlethal infections (19).

At present, we favor the notion that the ORF6 protein directly increases the efficiency of virus replication, assembly, or spread, since both viral RNA and protein levels are increased in rJ2.2.6-infected cells compared to those infected with rJ2.2.6^{KO} (Fig. 3). The ORF6 protein is detected throughout the cell and is membrane associated (Fig. 6), although it is present in highest concentrations in the perinuclear area, located in the same regions as the N and M proteins. The M protein is present in sites of virus assembly, while the N protein is localized almost entirely to sites of virus replication (7, 18). Thus, the ORF6 protein may have a direct role in enhancing virus replication or assembly. In SARS-CoV-infected cells, the ORF3a protein localizes to the perinuclear region and interacts with the E, M, and S proteins, while the ORF7a product is detected in the endoplasmic reticulum-Golgi region (21, 33).

The ORF3a protein is also detected in infectious virions (14, 40). Determining the relationship of ORF3a, -6, and -7a in SARS-CoV replication, assembly, and spread will clearly be important. Future efforts will also be directed at confirming the importance of the ORF6 protein in the context of intact SARS-CoV, particularly in virus-induced respiratory disease.

ACKNOWLEDGMENT

This research was supported in part by a grant from the NIH (PO1 AI060699).

REFERENCES

1. **Bergmann, C. C., Q. Yao, M. Lin, and S. A. Stohlman.** 1996. The JHM strain of mouse hepatitis virus induces a spike protein-specific D^b-restricted CTL response. J. Gen. Virol. **77:**315–325.
2. **Castro, R. F., and S. Perlman.** 1995. $CD8^+$ T-cell epitopes within the surface glycoprotein of a neurotropic coronavirus and correlation with pathogenicity. J. Virol. **69:**8127–8131.
3. **Chinese SARS Molecular Epidemiology Consortium.** 2004. Molecular evolution of the SARS coronavirus during the course of the SARS epidemic in China. Science **303:**1666–1669.
4. **Cinatl, J., B. Morgenstern, G. Bauer, P. Chandra, H. Rabenau, and H. W. Doerr.** 2003. Treatment of SARS with human interferons. Lancet **362:**293–294.
5. **Dandekar, A. A., and S. Perlman.** 2002. Virus-induced demyelination in nude mice is mediated by gamma delta T cells. Am. J. Pathol. **161:**1255–1263.
6. **de Groot-Mijnes, J. D., J. M. van Dun, R. G. van der Most, and R. J. de Groot.** 2005. Natural history of a recurrent feline coronavirus infection and the role of cellular immunity in survival and disease. J. Virol. **79:**1036–1044.
7. **Denison, M. R., W. J. Spaan, Y. van der Meer, C. A. Gibson, A. C. Sims, E. Prentice, and X. T. Lu.** 1999. The putative helicase of the coronavirus mouse hepatitis virus is processed from the replicase gene polyprotein and localizes in complexes that are active in viral RNA synthesis. J. Virol. **73:**6862–6871.
8. **Fleming, J. O., M. D. Trousdale, F. El-Zaatari, S. A. Stohlman, and L. P. Weiner.** 1986. Pathogenicity of antigenic variants of murine coronavirus JHM selected with monoclonal antibodies. J. Virol. **58:**869–875.
9. **Garlinghouse, L. E., Jr., A. L. Smith, and T. Holford.** 1984. The biological relationship of mouse hepatitis virus (MHV) strains and interferon: in vitro induction and sensitivities. Arch. Virol. **82:**19–29.
10. **Gorbalenya, A. E., E. J. Snijder, and W. J. Spaan.** 2004. Severe acute respiratory syndrome coronavirus phylogeny: toward consensus. J. Virol. **78:**7863–7866.
11. **Haring, J., and S. Perlman.** 2001. Mouse hepatitis virus. Curr. Opin. Microbiol. **4:**462–466.
12. **Hensley, L. E., L. E. Fritz, P. B. Jahrling, C. L. Karp, J. W. Huggins, and T. W. Geisbert.** 2004. Interferon-beta 1a and SARS coronavirus replication. Emerg. Infect. Dis. **10:**317–319.
13. **Houtman, J. J., and J. O. Fleming.** 1996. Dissociation of demyelination and viral clearance in congenitally immunodeficient mice infected with murine coronavirus JHM. J. Neurovirol. **2:**101–110.
14. **Ito, N., E. C. Mossel, K. Narayanan, V. L. Popov, C. Huang, T. Inoue, C. J. Peters, and S. Makino.** 2005. Severe acute respiratory syndrome coronavirus 3a protein is a viral structural protein. J. Virol. **79:**3182–3186.
15. **Kim, T. S., and S. Perlman.** 2003. Protection against CTL escape and clinical disease in a murine model of virus persistence. J. Immunol. **171:**2006–2013.
16. **Kim, T. S., and S. Perlman.** 2005. Virus-specific antibody, in the absence of T cells, mediates demyelination in mice infected with a neurotropic coronavirus. Am. J. Pathol. **166:**801–809.
17. **Kuo, L., G. J. Godeke, M. J. Raamsman, P. S. Masters, and P. J. Rottier.** 2000. Retargeting of coronavirus by substitution of the spike glycoprotein ectodomain: crossing the host cell species barrier. J. Virol. **74:**1393–1406.
18. **Lai, M. M. C., and D. Cavanagh.** 1997. The molecular biology of coronaviruses. Adv. Virus Res. **48:**1–100.
19. **Legge, K. L., and T. J. Braciale.** 2004. Diminished influenza specific $CD8^+$ T cell expansion and migration following lethal influenza virus infection. FASEB J. **18:**554.3.
20. **Mobley, J., G. Evans, M. O. Dailey, and S. Perlman.** 1992. Immune response to a murine coronavirus: identification of a homing receptor-negative $CD4^+$ T cell subset that responds to viral glycoproteins. Virology **187:**443–452.
21. **Nelson, C. A., A. Pekosz, C. A. Lee, M. S. Diamond, and D. H. Fremont.** 2005. Structure and intracellular targeting of the SARS-coronavirus Orf7a accessory protein. Structure **13:**75–85.
22. **Ontiveros, E., L. Kuo, P. S. Masters, and S. Perlman.** 2001. Inactivation of expression of gene 4 of mouse hepatitis virus strain JHM does not affect virulence in the murine CNS. Virology **290:**230–238.
23. **Peiris, J. S., Y. Guan, and K. Y. Yuen.** 2004. Severe acute respiratory syndrome. Nat. Med. **10:**S88–S97.
24. **Peiris, J. S., K. Y. Yuen, A. D. Osterhaus, and K. Stohr.** 2003. The severe acute respiratory syndrome. N. Engl. J. Med. **349:**2431–2441.
25. **Pewe, L., S. B. Heard, C. C. Bergmann, M. O. Dailey, and S. Perlman.** 1999. Selection of CTL escape mutants in mice infected with a neurotropic coronavirus: quantitative estimate of TCR diversity in the infected CNS. J. Immunol. **163:**6106–6113.
26. **Pewe, L., G. Wu, E. M. Barnett, R. Castro, and S. Perlman.** 1996. Cytotoxic T cell-resistant variants are selected in a virus-induced demyelinating disease. Immunity **5:**253–262.
27. **Sainz, B., Jr., E. C. Mossel, C. J. Peters, and R. F. Garry.** 2004. Interferon-beta and interferon-gamma synergistically inhibit the replication of severe acute respiratory syndrome-associated coronavirus (SARS-CoV). Virology **329:**11–17.
28. **Song, H. D., C. C. Tu, G. W. Zhang, S. Y. Wang, K. Zheng, L. C. Lei, Q. X. Chen, Y. W. Gao, H. Q. Zhou, H. Xiang, H. J. Zheng, S. W. Chern, F. Cheng, C. M. Pan, H. Xuan, S. J. Chen, H. M. Luo, D. H. Zhou, Y. F. Liu, J. F. He, P. Z. Qin, L. H. Li, Y. Q. Ren, W. J. Liang, Y. D. Yu, L. Anderson, M. Wang, R. H. Xu, X. W. Wu, H. Y. Zheng, J. D. Chen, G. Liang, Y. Gao, M. Liao, L. Fang, L. Y. Jiang, H. Li, F. Chen, B. Di, L. J. He, J. Y. Lin, S. Tong, X. Kong, L. Du, P. Hao, H. Tang, A. Bernini, X. J. Yu, O. Spiga, Z. M. Guo, H. Y. Pan, W. Z. He, J. C. Manuguerra, A. Fontanet, A. Danchin, N. Niccolai, Y. X. Li, C. I. Wu, and G. P. Zhao.** 2005. Cross-host evolution of severe acute respiratory syndrome coronavirus in palm civet and human. Proc. Natl. Acad. Sci. USA **102:**2430–2435.
29. **Spiegel, M., A. Pichlmair, L. Martinez-Sobrido, J. Cros, A. Garcia-Sastre, O. Haller, and F. Weber.** 2005. Inhibition of beta interferon induction by severe acute respiratory syndrome coronavirus suggests a two-step model for activation of interferon regulatory factor 3. J. Virol. **79:**2079–2086.
30. **Stohlman, S. A., C. C. Bergmann, and S. Perlman.** 1998. Mouse hepatitis virus, p. 537–557. *In* R. Ahmed and I. Chen (ed.), Persistent viral infections. John Wiley & Sons, Ltd., New York, N.Y.
31. **Stroher, U., A. DiCaro, Y. Li, J. E. Strong, F. Aoki, F. Plummer, S. M. Jones, and H. Feldmann.** 2004. Severe acute respiratory syndrome-related coronavirus is inhibited by interferon-alpha. J. Infect. Dis. **189:**1164–1167.
32. **Subbarao, K., J. McAuliffe, L. Vogel, G. Fahle, S. Fischer, K. Tatti, M. Packard, W. J. Shieh, S. Zaki, and B. Murphy.** 2004. Prior infection and passive transfer of neutralizing antibody prevent replication of severe acute respiratory syndrome coronavirus in the respiratory tract of mice. J. Virol. **78:**3572–3577.
33. **Tan, Y. J., E. Teng, S. Shen, T. H. Tan, P. Y. Goh, B. C. Fielding, E. E. Ooi, H. C. Tan, S. G. Lim, and W. Hong.** 2004. A novel severe acute respiratory syndrome coronavirus protein, U274, is transported to the cell surface and undergoes endocytosis. J. Virol. **78:**6723–6734.
34. **Turner, B. C., E. M. Hemmila, N. Beauchemin, and K. V. Holmes.** 2004. Receptor-dependent coronavirus infection of dendritic cells. J. Virol. **78:**5486–5490.
35. **Wang, F., J. O. Fleming, and M. M. C. Lai.** 1992. Sequence analysis of the spike protein gene of murine coronavirus variants: study of genetic sites affecting neuropathogenicity. Virology **186:**742–749.
36. **Wu, G. F., A. A. Dandekar, L. Pewe, and S. Perlman.** 2000. CD4 and CD8 T cells have redundant but not identical roles in virus-induced demyelination. J. Immunol. **165:**2278–2286.
37. **Wu, G. F., and S. Perlman.** 1999. Macrophage infiltration, but not apoptosis, is correlated with immune-mediated demyelination following murine infection with a neurotropic coronavirus. J. Virol. **73:**8771–8780.
38. **Xue, S., A. Jaszewski, and S. Perlman.** 1995. Identification of a $CD4^+$ T cell epitope within the M protein of a neurotropic coronavirus. Virology **208:**173–179.
39. **Yilla, M., B. H. Harcourt, C. J. Hickman, M. McGrew, A. Tamin, C. S. Goldsmith, W. J. Bellini, and L. J. Anderson.** 2005. SARS-coronavirus replication in human peripheral monocytes/macrophages. Virus Res. **107:**93–101.
40. **Zeng, R., R. F. Yang, M. D. Shi, M. R. Jiang, Y. H. Xie, H. Q. Ruan, X. S. Jiang, L. Shi, H. Zhou, L. Zhang, X. D. Wu, Y. Lin, Y. Y. Ji, L. Xiong, Y. Jin, E. H. Dai, X. Y. Wang, B. Y. Si, J. Wang, H. X. Wang, C. E. Wang, Y. H. Gan, Y. C. Li, J. T. Cao, J. P. Zuo, S. F. Shan, E. Xie, S. H. Chen, Z. Q. Jiang, X. Zhang, Y. Wang, G. Pei, B. Sun, and J. R. Wu.** 2004. Characterization of the 3a protein of SARS-associated coronavirus in infected Vero E6 cells and SARS patients. J. Mol. Biol. **341:**271–279.